energies

MDPI

Article

Voltage Modulated DPC Strategy of DFIG Using Extended Power Theory under Unbalanced Grid Voltage Conditions

Peng Cheng [1], Chao Wu [2,*], Fuwei Ning [1] and Jing He [3]

[1] China Institute of Energy and Transportation Integrated Development, North China Electric Power University, Beijing 102206, China; P.Cheng@ncepu.edu.cn (P.C.); fw.ning@ncepu.edu.cn (F.N.)
[2] Department of Energy Technology, Aalborg University, DK 9220 Aalborg, Denmark
[3] State Key Laboratory of Operation and Control of Renewable Energy & Storage Systems, China Electric Power Research Institute, Beijing 100192, China; hejing@epri.sgcc.com.cn
* Correspondence: cwu@et.aau.dk

Received: 14 September 2020; Accepted: 17 November 2020; Published: 20 November 2020



Abstract: This paper develops a voltage modulated direct power control (VM-DPC) strategy of a doubly fed induction generator (DFIG) using extended power theory under unbalanced grid voltage conditions. By introducing the modulated voltage of the active and reactive powers and the non-linear VM controller, the proposed VM-DPC strategy enables the generator dynamics to change from the time-varying differential equations into the time-invariant ones. Then, in order to deal with the voltage unbalance, three available power feedbacks, a combination of real active power and extended reactive power, a combination of extended active power and real reactive power, a combination of extended active power and extended reactive power, are developed. Together with a conventional controller (PI + R and feedforwards) and a non-linear VM controller, the power feedbacks are well controlled to track their references with the achievement of the constant active power, the constant reactive power and the balanced stator current. The main advantage of the VM-DPC strategy is the introduction of the modulated voltage and the non-linear VM controller making the generator dynamics time-invariant, which is easy for applying various control methods. Furthermore, the application of extended power can avoid the sequence extractions and the power compensations under unbalanced grid voltage. Finally, the simulation results demonstrate the effectiveness of the developed VM-DPC strategy.

Keywords: direct power control; doubly fed induction generator; extended power theory; voltage modulated; unbalanced grid voltage

1. Introduction

In recent years, wind power generation has been rapidly developing among different types of renewable power generation. The doubly fed induction generators (DFIGs) are widely employed in wind farms, due to the attractive merits of variable-speed operation, power decoupling control and lower converter rating [1,2]. However, since wind farms are usually in a rural area with long transmission lines, the voltage unbalance has become a common disturbance [3,4]. For dealing with this disturbance, various solutions have been designed on vector-oriented control (VOC) and direct power control (DPC).

One classical VOC is implemented in the positive and negative synchronous reference frame, where the unbalanced ac signals in the stationary reference frame are transferred to the DC signals in the positive and negative synchronous reference frame [5,6], respectively. Then, dual proportional-integral

(PI) controllers implemented in each synchronous reference frame can effectively regulate the positive- and negative-sequence current. Since it is oriented with the grid voltage, during unbalanced voltage, several improved phase-locked loops (PLLs) are employed for grid synchronization [7], including notch filter (NF)–PLL, double synchronous reference frame (DSRF)-PLL and delayed signal cancellation (DSC)–PLL. However, these advanced PLLs would make negative impacts on system stability and must be carefully designed with a higher complexity of implementation [8,9]. Another classical VOC is implemented in the stationary reference frame and proportional plus resonant (P+R) controllers are employed as AC controllers [10,11]. In the stationary reference frame, the current reference is generated based on the instantaneous power theory. However, the voltage unbalance would introduce more harmonics in the current reference [12,13] and then the DFIG operation would be jeopardized with a highly distorted current and undesired power pulsations.

As a powerful alternative method to VOC, DPC has been widely studied in [14–23] without the current control loop and the PLL. The conventional lookup-table DPC with hysteresis shows advantages of fast dynamic response and simple implementation, but it would produce large power ripples with variable switching frequencies due to the hysteresis comparator. To address this, one class of improved DPC strategies is based on model predictive control (MPC), called MPC-DPC, which is implemented with various cost functions [14]. By minimizing the designed cost function, multiple-vector-based MPC-DPC is developed to achieve the constant switching frequency in [15,16]. However, this nonlinear control derived from predictive control is complicated with a greater computational burden. Another class of improved DPC strategies is based on space vector modulation (SVM), namely SVM-DPC [17,18]. In this category, the voltage vector is synthesized by pulse width modulation instead of the cost function and corresponding selection in MPC-DPC. To deal with the voltage unbalance, the flexible power compensation terms are added to the original power reference for achieving adjustable current unbalance and power ripples in [19,20]. However, the power compensation terms are calculated on positive- and negative-sequence voltage/current. For removing positive- and negative-sequence extraction, a sliding-mode-control (SMC)-DPC is developed based on extended power theory for generating hybrid power reference in [21]. However, the nonlinear SMC regulator is very complicated to guarantee the convergence to its equilibrium point. Recently, in [22,23], a grid voltage modulation-based DPC is proposed for voltage source converters with good steady-state performance and dynamic response. However, this method required the assumption that the grid voltage is balanced, which restricts its application under unbalanced grid voltage conditions. Consequently, further studies need to be conducted for enhanced operation under unbalanced grid voltage conditions.

Thus, the motivation of this paper is to develop a voltage modulated (VM)-DPC strategy of DFIGs under unbalanced grid voltage conditions. In this VM-DPC strategy, the modulated voltages of the active and reactive powers are introduced as the controlled variables and then a non-linear controller is proposed on the basis of the generator model. By these means, the time-varying power dynamics of the generator change into the time-invariant ones, which enables various control methods to be easily applied. Then, under unbalanced grid voltage conditions, combining the classical and extended power theory, three available power feedbacks are designed. Together with the conventional controller (PI+R and feedforwards) and the non-linear VM controller, the available power feedbacks are effectively controlled to track their references with the achievement of ensuring constant active power, constant reactive power and balanced stator current. The main advantages of the developed VM-DPC strategy can be summarized as: (1) the introduction of the modulated voltage and the non-linear VM controller causing the generator dynamics to be the time-invariant ones for easily applying various control methods; (2) the lack of the sequence extractions and the power compensations under unbalanced grid voltage conditions with a simpler implementation. Finally, the effectiveness of the developed VM-DPC strategy is verified.

This paper is organized as follows. Section 2 gives the mathematical model of a DFIG. In Section 3, the available feedback powers, consisting of the classical and extended powers, are designed for the

defined control targets. Then, the detailed implementation of the VM-DPC strategy is described. The simulation results are discussed in Section 4. Finally, Section 5 summarizes the conclusions.

2. Mathematic Model

In order to analyze the characteristic of DFIG under an unbalanced grid, the mathematical model is established in this section. Furthermore, the extended power theory is also introduced, and the relationship between real power and extended power is revealed in this Section to give a basis for the proposed control strategy in the next section.

2.1. Power Analysis

The grid condition in this study is assumed to be unbalanced without zero-sequence voltage and harmonics in a three-phase three-wire system. Accordingly, the voltages and currents contain both positive- and negative-sequence components, which can be expressed in the stationary reference frame as,

$$\begin{cases} u_{s\alpha} = u_{s\alpha+} + u_{s\alpha-} = U_{s+}\cos\left(\omega_g t + \theta_{u+}\right) + U_{s-}\cos\left(-\omega_g t + \theta_{u-}\right) \\ u_{s\beta} = u_{s\beta+} + u_{g\beta-} = U_{s+}\sin\left(\omega_g t + \theta_{u+}\right) + U_{s-}\sin\left(-\omega_g t + \theta_{u-}\right) \end{cases} \tag{1}$$

$$\begin{cases} i_{s\alpha} = i_{s\alpha+} + i_{s\alpha-} = I_{s+}\cos\left(\omega_g t + \theta_{i+}\right) + I_{s-}\cos\left(-\omega_g t + \theta_{i-}\right) \\ i_{s\beta} = i_{s\beta+} + i_{g\beta-} = I_{s+}\sin\left(\omega_g t + \theta_{i+}\right) + I_{s-}\sin\left(-\omega_g t + \theta_{i-}\right) \end{cases} \tag{2}$$

where $u_{s\alpha\beta}$ and $i_{s\alpha\beta}$ are the DFIG stator voltages and currents, subscripts +, − refer to the positive- and negative-sequence components, U_{s+}, U_{s-} and I_{s+}, I_{s-} are the amplitudes of positive- and negative-sequence voltages and currents, θ_{u+}, θ_{u-} and θ_{i+}, θ_{i-} are the initial phase angle of positive- and negative-sequence voltages and currents, ω_g is the grid angular frequency, respectively.

Based on the instantaneous power theory, the apparent powers of the DFIG stator can be calculated as,

$$\boldsymbol{S}_s = 1.5\boldsymbol{U}^*_{s\alpha\beta}\boldsymbol{I}_{s\alpha\beta} = P_s - jQ_s \tag{3}$$

where $\boldsymbol{S}_s$, P_s and Q_s are the apparent power, the active power and the reactive power, superscript * denotes the conjugate of the complex phasors, respectively.

Then, under unbalanced grid voltage conditions, the classical active and reactive powers, containing both the average part and the oscillating part, are calculated as,

$$\begin{cases} P_s = 1.5\mathrm{Re}\left[\boldsymbol{U}^*_{s\alpha\beta}\boldsymbol{I}_{s\alpha\beta}\right] = P_{s_0} + P_{s_i2} + P_{s_u2} \\ Q_s = -1.5\mathrm{Im}\left[\boldsymbol{U}^*_{s\alpha\beta}\boldsymbol{I}_{s\alpha\beta}\right] = Q_{s_0} + Q_{s_i2} + Q_{s_u2} \end{cases} \tag{4}$$

where Re and Im refer to the real and imaginary parts of the apparent power,

$$\begin{cases} P_{s_0} = 1.5\left(u_{s\alpha+}i_{s\alpha+} + u_{s\beta+}i_{s\beta+} + u_{s\alpha-}i_{s\alpha-} + u_{s\beta}i_{s\beta-}\right) \\ = 1.5[U_{s+}I_{s+}\cos(\theta_{u+} - \theta_{i+}) + U_{s-}I_{s-}\cos(\theta_{u-} - \theta_{i-})] \\ P_{s_i2} = 1.5\left(u_{s\alpha+}i_{s\alpha-} + u_{s\beta+}i_{s\beta-}\right) = 1.5U_{s+}I_{s-}\cos\left(2\omega_g t + \theta_{u+} - \theta_{i-}\right) \\ P_{s_u2} = 1.5\left(u_{s\alpha-}i_{s\alpha+} + u_{s\beta-}i_{s\beta+}\right) = 1.5U_{s-}I_{s+}\cos\left(-2\omega_g t + \theta_{u-} - \theta_{i+}\right) \end{cases} \tag{5}$$

$$\begin{cases} Q_{s_0} = 1.5\left(u_{s\beta+}i_{s\alpha+} - u_{s\alpha+}i_{s\beta+} + u_{s\beta-}i_{s\alpha-} - u_{s\alpha-}i_{s\beta-}\right) \\ = 1.5[U_{s+}I_{s+}\sin(\theta_{u+} - \theta_{i+}) + U_{s-}I_{s-}\sin(\theta_{u-} - \theta_{i-})] \\ Q_{s_i2} = 1.5\left(u_{s\beta+}i_{s\alpha-} - u_{s\alpha+}i_{s\beta-}\right) = 1.5U_{s+}I_{s-}\sin\left(2\omega_g t + \theta_{u+} - \theta_{i-}\right) \\ Q_{s_u2} = 1.5\left(u_{s\beta-}i_{s\alpha+} - u_{s\alpha-}i_{s\beta+}\right) = 1.5U_{s-}I_{s+}\sin\left(-2\omega_g t + \theta_{u-} - \theta_{i+}\right) \end{cases} \tag{6}$$

Based on the extended power theory, the extended active and reactive powers are calculated based on a lagged 90° (1/4 fundamental period) voltage. Then, the 90° lagged α- and β-axis voltages are obtained as,

$$\begin{cases} u'_{s\alpha+} = U_{s+}\cos\left(\omega_g t + \theta_{u+} - \pi/2\right) = U_{s+}\sin\left(\omega_g t + \theta_{u+}\right) = u_{s\beta+} \\ u'_{s\beta+} = U_{s+}\sin\left(\omega_g t + \theta_{u+} - \pi/2\right) = -U_{s+}\cos\left(\omega_g t + \theta_{u+}\right) = -u_{s\alpha+} \\ u'_{s\alpha-} = U_{s-}\cos\left(-\omega_g t + \theta_{u-} + \pi/2\right) = -U_{s-}\sin\left(-\omega_g t + \theta_{u-}\right) = -u_{s\beta-} \\ u'_{s\beta-} = U_{s-}\sin\left(-\omega_g t + \theta_{u-} + \pi/2\right) = U_{s-}\cos\left(-\omega_g t + \theta_{u-}\right) = u_{s\alpha-} \end{cases} \tag{7}$$

where superscript ' refers to the delay signals by one quarter of the fundamental period.

Accordingly, the extended active and reactive powers are calculated as,

$$S_{s_ex} = 1.5\boldsymbol{U}'^{*}_{s\alpha\beta}\boldsymbol{I}_{s\alpha\beta} = Q_{s_ex} + jP_{s_ex} \tag{8}$$

where S_{s_ex}, P_{s_ex} and Q_{s_ex} are the extended apparent power, the extended active power and the extended reactive power, respectively.

During network unbalance, the extended active and reactive powers also contain both the average part and the oscillating part, which are calculated as,

$$\begin{cases} P_{s_ex} = 1.5\mathrm{Im}\left[\boldsymbol{U}'^{*}_{s\alpha\beta}\boldsymbol{I}_{s\alpha\beta}\right] = P_{s_ex0} + P_{s_exi2} + P_{s_exu2} \\ Q_{s_ex} = 1.5\mathrm{Re}\left[\boldsymbol{U}'^{*}_{s\alpha\beta}\boldsymbol{I}_{s\alpha\beta}\right] = Q_{s_ex0} + Q_{s_exi2} + Q_{s_exu2} \end{cases} \tag{9}$$

where

$$\begin{cases} P_{s_ex0} = 1.5\left(u_{s\alpha+}i_{s\alpha+} + u_{s\beta+}i_{s\beta+} - u_{s\alpha-}i_{s\alpha-} - u_{s\beta}i_{s\beta-}\right) \\ \quad\quad = 1.5[U_{s+}I_{s+}\cos(\theta_{u+} - \theta_{i+}) - U_{s-}I_{s-}\cos(\theta_{u-} - \theta_{i-})] \\ P_{s_exi2} = 1.5\left(u_{g\alpha+}i_{\alpha-} + u_{g\beta+}i_{\beta-}\right) = 1.5U_{s+}I_{s-}\cos\left(2\omega_g t + \theta_{u+} - \theta_{i-}\right) \\ P_{s_exu2} = 1.5\left(-u_{g\alpha-}i_{\alpha+} - u_{g\beta-}i_{\beta+}\right) = -1.5U_{s-}I_{s+}\cos\left(-2\omega_g t + \theta_{u-} - \theta_{i+}\right) \end{cases} \tag{10}$$

$$\begin{cases} Q_{s_ex0} = 1.5\left(u_{s\beta+}i_{s\alpha+} - u_{s\alpha+}i_{s\beta+} - u_{s\beta-}i_{s\alpha-} + u_{s\alpha-}i_{s\beta-}\right) \\ \quad\quad = 1.5[U_{s+}I_{s+}\sin(\theta_{u+} - \theta_{i+}) - U_{s-}I_{s-}\sin(\theta_{u-} - \theta_{i-})] \\ Q_{s_exi2} = 1.5\left(u_{s\beta+}i_{s\alpha-} - u_{s\alpha+}i_{s\beta-}\right) = 1.5U_{s+}I_{s-}\sin\left(2\omega_g t + \theta_{u+} - \theta_{i-}\right) \\ Q_{s_exu2} = 1.5\left(u_{s\alpha-}i_{s\beta+} - u_{s\beta-}i_{s\alpha+}\right) = -1.5U_{s-}I_{s+}\sin\left(-2\omega_g t + \theta_{u-} - \theta_{i+}\right) \end{cases} \tag{11}$$

As seen, the oscillating parts of the classical and extended active and reactive powers caused by the positive-sequence voltage and the negative-sequence current are equal to each other, while the oscillating parts of the classical and extended active and reactive powers caused by the negative-sequence voltage and the positive-sequence current are opposite. Meanwhile, since the average active and reactive powers produced by the negative-sequence voltages and currents are relatively small, they can be approximately regarded as null. This means that the average parts of both the classical and extended active/reactive powers are equal to each other. Consequently, based on the previous analysis, the following equation can be obtained as,

$$\begin{cases} P_{s_0} \approx P_{s_ex0}, Q_{s_0} \approx Q_{s_ex0} \\ P_{s_i2} = P_{s_exi2}, P_{s_u2} = -P_{s_exu2} \\ Q_{s_i2} = Q_{s_exi2}, Q_{s_u2} = -Q_{s_exu2} \end{cases} \tag{12}$$

2.2. DFIG Model

Accordingly, based on Equations (1) and (7), the differential equations of the α- and β-axis voltage, containing both the positive- and negative-sequence components, are obtained as

$$\begin{cases} \frac{\mathrm{d}u_{s\alpha}}{\mathrm{d}t} = -\omega_g U_{s+}\sin\left(\omega_g t + \theta_{u+}\right) + \omega_g U_{s-}\sin\left(-\omega_g t + \theta_{u-}\right) = -\omega_g\left(u'_{s\alpha+} + u'_{s\alpha-}\right) = -\omega_g u'_{s\alpha} \\ \frac{\mathrm{d}u_{s\beta}}{\mathrm{d}t} = \omega_g U_{s+}\cos\left(\omega_g t + \theta_{u+}\right) - \omega_g U_{s-}\cos\left(-\omega_g t + \theta_{u-}\right) = -\omega_g\left(u'_{s\beta+} + u'_{s\beta-}\right) = -\omega_g u'_{s\beta} \end{cases} \tag{13}$$

For a complex vector expression, Equation (13) is rewritten as,

$$\frac{\mathrm{d}}{\mathrm{d}t}\boldsymbol{U}^*_{sa\beta} = -\omega_g \boldsymbol{U}'^*_{sa\beta} \tag{14}$$

where $\boldsymbol{U}_{sa\beta}$ is the voltage vector and given as,

$$\boldsymbol{U}_{s\alpha\beta} = u_{s\alpha} + \mathrm{j}\cdot u_{s\beta} \tag{15}$$

Then, based on Equation (3), the dynamics of the active and reactive powers of a DFIG are obtained as,

$$\begin{aligned} \tfrac{\mathrm{d}}{\mathrm{d}t}\boldsymbol{S} &= 1.5\boldsymbol{U}^*_{s\alpha\beta}\tfrac{\mathrm{d}}{\mathrm{d}t}\boldsymbol{I}_{s\alpha\beta} + 1.5\boldsymbol{I}_{s\alpha\beta}\tfrac{\mathrm{d}}{\mathrm{d}t}\boldsymbol{U}^*_{s\alpha\beta} = 1.5\boldsymbol{U}^*_{s\alpha\beta}\tfrac{\mathrm{d}}{\mathrm{d}t}\boldsymbol{I}_{s\alpha\beta} - \omega_g 1.5\boldsymbol{U}'^*_{sa\beta}\boldsymbol{I}_{s\alpha\beta} \\ &= 1.5\boldsymbol{U}^*_{s\alpha\beta}\tfrac{\mathrm{d}}{\mathrm{d}t}\boldsymbol{I}_{s\alpha\beta} - \omega_g \boldsymbol{S}_{s_ex} \end{aligned} \tag{16}$$

In order to give a more intuitive representation of DFIG model, the equivalent circuit of DFIG in the stationary frame is shown in Figure 1.

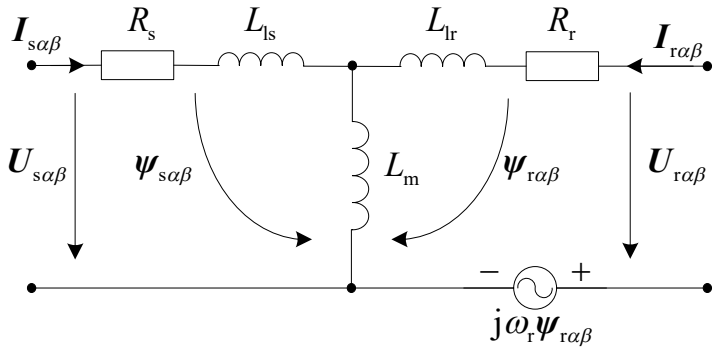


Figure 1. Doubly fed induction generator (DFIG) equivalent circuit in the stationary reference frame.

As can be seen in Figure 1, the dynamics of the DFIG voltage and flux linkages are given as,

$$\begin{cases} \boldsymbol{U}_{sa\beta} = R_s\boldsymbol{I}_{sa\beta} + \frac{d\boldsymbol{\psi}_{sa\beta}}{dt} \\ \boldsymbol{U}_{ra\beta} = R_r\boldsymbol{I}_{ra\beta} + \frac{d\boldsymbol{\psi}_{ra\beta}}{dt} - \mathrm{j}\omega_r\boldsymbol{\psi}_{ra\beta} \end{cases} \tag{17}$$

$$\begin{cases} \boldsymbol{\psi}_{sa\beta} = L_s\boldsymbol{I}_{sa\beta} + L_m\boldsymbol{I}_{ra\beta} \\ \boldsymbol{\psi}_{ra\beta} = L_m\boldsymbol{I}_{sa\beta} + L_r\boldsymbol{I}_{ra\beta} \end{cases} \tag{18}$$

where R_s and R_r are the stator and rotor resistances, ω_r is the rotor angular frequency, L_m is the mutual inductance, L_{ls} and L_{lr} are the stator and rotor leakage inductances, $L_s = L_m + L_{ls}$ and $L_r = L_m + L_{lr}$ are the stator and rotor self-inductances, respectively.

According to Equation (18), the rotor flux linkage and current can be also expressed as,

$$\boldsymbol{\psi}_{ra\beta} = \frac{L_r}{L_m}\boldsymbol{\psi}_{sa\beta} - \frac{\sigma L_r L_s}{L_m}\boldsymbol{I}_{sa\beta} \tag{19}$$

$$\boldsymbol{I}_{\mathrm{ra}\beta} = \frac{\boldsymbol{\psi}_{\mathrm{sa}\beta}}{L_{\mathrm{m}}} - \frac{L_{\mathrm{s}}}{L_{\mathrm{m}}}\boldsymbol{I}_{\mathrm{sa}\beta} \tag{20}$$

where $\sigma = 1 - {L_{\mathrm{m}}}^2/(L_{\mathrm{s}}\,L_{\mathrm{r}})$ is the leakage factor.

Then, submitting Equations (19) and (20) into the dynamics of the DFIG rotor voltage in Equation (17), the dynamics of the DFIG stator current are obtained as,

$$\begin{aligned}\tfrac{\sigma L_{\mathrm{r}}L_{\mathrm{s}}}{L_{\mathrm{m}}}\tfrac{\mathrm{d}}{\mathrm{d}t}\boldsymbol{I}_{s\alpha\beta} &= \tfrac{R_{\mathrm{r}}-\mathrm{j}\omega_{\mathrm{r}}L_{\mathrm{r}}}{L_{\mathrm{m}}}\boldsymbol{\psi}_{s\alpha\beta} + \tfrac{L_{\mathrm{r}}}{L_{\mathrm{m}}}\tfrac{\mathrm{d}}{\mathrm{d}t}\boldsymbol{\psi}_{s\alpha\beta} - \tfrac{L_{\mathrm{s}}}{L_{\mathrm{m}}}(R_{\mathrm{r}} + \mathrm{j}\omega_{\mathrm{r}}\sigma L_{\mathrm{r}})\boldsymbol{I}_{s\alpha\beta} - \boldsymbol{U}_{r\alpha\beta}\\ &= \tfrac{L_{\mathrm{r}}}{L_{\mathrm{m}}}\Big\{\boldsymbol{U}_{s\alpha\beta} + \Big(\tfrac{R_{\mathrm{r}}}{L_{\mathrm{r}}} - \mathrm{j}\omega_{\mathrm{r}}\Big)\boldsymbol{\psi}_{s\alpha\beta}\Big\} - \tfrac{L_{\mathrm{r}}L_{\mathrm{s}}}{L_{\mathrm{m}}}\Big(\tfrac{R_{\mathrm{s}}}{L_{\mathrm{s}}} + \tfrac{R_{\mathrm{r}}}{L_{\mathrm{r}}} - \mathrm{j}\omega_{\mathrm{r}}\sigma\Big)\boldsymbol{I}_{s\alpha\beta} - \boldsymbol{U}_{r\alpha\beta}\end{aligned} \tag{21}$$

In practice, the actual grid angular frequency would vary around the nominal value in an allowed narrow range, such as ±0.5 Hz [24] and ±1.0 Hz [25]. For a simplified implementation, a nominal angular frequency ω_1 is used instead of the actual one ω_{g} in Equation (21). Meanwhile, the rotor resistance R_{r} and the stator resistance R_{s} is far lower than the rotor and stator inductance, thus, the term $R_{\mathrm{r}}/L_{\mathrm{r}}$ and $R_{\mathrm{s}}/L_{\mathrm{s}}$ can be assumed to be null in Equation (21). Based on the analysis, the dynamics of the stator current is simplified as,

$$\frac{\sigma L_{\mathrm{r}}L_{\mathrm{s}}}{L_{\mathrm{m}}}\frac{\mathrm{d}}{\mathrm{d}t}\boldsymbol{I}_{s\alpha\beta} = \frac{L_{\mathrm{r}}}{L_{\mathrm{m}}}\Big(\boldsymbol{U}_{s\alpha\beta} - \mathrm{j}\omega_{\mathrm{r}}\boldsymbol{\psi}_{s\alpha\beta}\Big) + \mathrm{j}\frac{\omega_{\mathrm{r}}\sigma L_{\mathrm{r}}L_{\mathrm{s}}}{L_{\mathrm{m}}}\boldsymbol{I}_{s\alpha\beta} - \boldsymbol{U}_{r\alpha\beta} \tag{22}$$

where $\omega_1 = 100\pi$ rad/s is the nominal grid angular frequency.

Then, submitting Equation (22) into Equation (16), the dynamics of the active and reactive powers of a DFIG are rewritten as,

$$\frac{\sigma L_{\mathrm{r}}L_{\mathrm{s}}}{L_{\mathrm{m}}}\frac{\mathrm{d}}{\mathrm{d}t}\boldsymbol{S} = 1.5\boldsymbol{U}^{*}_{\mathrm{s}\alpha\beta}\Big[\frac{L_{\mathrm{r}}}{L_{\mathrm{m}}}\boldsymbol{U}_{s\alpha\beta} - \boldsymbol{U}_{r\alpha\beta}\Big] - \mathrm{j}1.5\omega_{\mathrm{r}}\boldsymbol{U}^{*}_{\mathrm{s}\alpha\beta}\boldsymbol{\psi}_{s\alpha\beta} + \mathrm{j}\frac{\omega_{\mathrm{r}}\sigma L_{\mathrm{r}}L_{\mathrm{s}}}{L_{\mathrm{m}}}\boldsymbol{S}_{\mathrm{s}} - \omega_1\frac{\sigma L_{\mathrm{r}}L_{\mathrm{s}}}{L_{\mathrm{m}}}\boldsymbol{S}_{\mathrm{s_ex}} \tag{23}$$

For clear statements and calculations, the scalar expression of Equation (23) is given as,

$$\tfrac{\sigma L_{\mathrm{r}}L_{\mathrm{s}}}{L_{\mathrm{m}}}\tfrac{\mathrm{d}}{\mathrm{d}t}\begin{bmatrix} P_{\mathrm{s}} \\ Q_{\mathrm{s}}\end{bmatrix} = 1.5\begin{bmatrix} u_{\mathrm{s}\alpha} & u_{\mathrm{s}\beta} \\ u_{\mathrm{s}\beta} & -u_{\mathrm{s}\alpha}\end{bmatrix}\Big\{\tfrac{L_{\mathrm{r}}}{L_{\mathrm{m}}}\begin{bmatrix} u_{\mathrm{s}\alpha} \\ u_{\mathrm{s}\beta}\end{bmatrix} - \begin{bmatrix} u_{\mathrm{r}\alpha} \\ u_{\mathrm{r}\beta}\end{bmatrix}\Big\} - \tfrac{\sigma L_{\mathrm{r}}L_{\mathrm{s}}}{L_{\mathrm{m}}}\begin{bmatrix} \omega_1 P_{\mathrm{s_ex}} + \omega_{\mathrm{r}}Q_{\mathrm{s}} \\ \omega_1 Q_{\mathrm{s_ex}} - \omega_{\mathrm{r}}P_{\mathrm{s}}\end{bmatrix} + 1.5\omega_{\mathrm{r}}\begin{bmatrix} u_{\mathrm{s}\beta} & u_{\mathrm{s}\alpha} \\ u_{\mathrm{s}\alpha} & -u_{\mathrm{s}\beta}\end{bmatrix}\begin{bmatrix} \psi_{\mathrm{s}\alpha} \\ \psi_{\mathrm{s}\beta}\end{bmatrix} \tag{24}$$

It is noted in Equation (24) that the dynamics of the active and reactive powers of a DFIG have the ac voltage-related coefficients, which makes it a non-linear time-varying system. In order to change the time-varying system into the time-invariant one, the modulated voltages of the active and reactive powers are defined as,

$$\begin{bmatrix} u_{\mathrm{P}} \\ u_{\mathrm{Q}}\end{bmatrix} = \frac{L_{\mathrm{r}}}{L_{\mathrm{m}}}\begin{bmatrix} U^2_{\mathrm{sm}} \\ 0\end{bmatrix} - \begin{bmatrix} u_{\mathrm{s}\alpha} & u_{\mathrm{s}\beta} \\ u_{\mathrm{s}\beta} & -u_{\mathrm{s}\alpha}\end{bmatrix}\begin{bmatrix} u_{\mathrm{r}\alpha} \\ u_{\mathrm{r}\beta}\end{bmatrix} \tag{25}$$

where u_{P} and u_{q} are the modulated voltages of the active and reactive powers, U_{sm} is the amplitude of the stator voltage and calculated as

$$U_{\mathrm{sm}} = \sqrt{u^2_{s\alpha} + u^2_{s\beta}} \tag{26}$$

Due to the introduction of the modulated voltages of the active and reactive powers, the differential equation of the active and reactive powers of a DFIG is simplified as,

$$\frac{\sigma L_{\mathrm{r}}L_{\mathrm{s}}}{L_{\mathrm{m}}}\frac{\mathrm{d}}{\mathrm{d}t}\begin{bmatrix} P \\ Q\end{bmatrix} = 1.5\begin{bmatrix} u_{\mathrm{P}} \\ u_{\mathrm{Q}}\end{bmatrix} - \frac{\sigma L_{\mathrm{r}}L_{\mathrm{s}}}{L_{\mathrm{m}}}\begin{bmatrix} \omega_1 P_{\mathrm{s_ex}} + \omega_{\mathrm{r}}Q_{\mathrm{s}} \\ \omega_1 Q_{\mathrm{s_ex}} - \omega_{\mathrm{r}}P_{\mathrm{s}}\end{bmatrix} + 1.5\omega_{\mathrm{r}}\begin{bmatrix} u_{\mathrm{s}\beta} & u_{\mathrm{s}\alpha} \\ u_{\mathrm{s}\alpha} & -u_{\mathrm{s}\beta}\end{bmatrix}\begin{bmatrix} \psi_{\mathrm{s}\alpha} \\ \psi_{\mathrm{s}\beta}\end{bmatrix} \tag{27}$$

As seen from Equation (27), the time-varying differential equation of the active and reactive powers of a DFIG is converted into the time-invariant constant coefficient-related one, due to the introduction of the modulated voltage of the active and reactive powers. This merit enables various control methods to be easily applied here. Besides, all the aforementioned calculations are in the

stationary reference frame, where the need for the PLL is completely avoided in the VM-DPC strategy for a simple implementation.

3. Control System

Based on the power analysis and the mathematical model of DFIG, the relationship between the power ripple, harmonic currents, and the extended power is built in this section. Then, three different control targets under an unbalanced grid are elaborated. Furthermore, the system implementation of the control strategy is presented to give a more intuitive understanding of the developed VM-DPC strategy.

3.1. Control Targets

The voltage unbalance would produce the current unbalance/harmonics, the power pulsations and the torque ripples and then the DFIG operation tends to worsen. Thus, the VM-DPC with unbalanced control is necessitated for the sake of reinforcing the generator performance under unbalanced grid voltage conditions. From the generator operation point of view, three control targets are defined as,

Target I: To remove the oscillating active power.
Target II: To remove the oscillating reactive power and also the oscillating torque.
Target III: To operate with balanced stator currents.

As with Target I, the oscillating parts of the active power are controlled to be zero, thus, the active power is constant with the fact that $P_{s_i2} + P_{s_u2} = 0$. Then, based on Equation (5), the amplitude and phase angle of the negative-sequence current are obtained as,

$$\begin{cases} I_{s-} = U_{s-} I_{s+} / U_{s+} \\ \theta_{i-} = \theta_{u+} - \theta_{i+} + \theta_{u-} + \pi \end{cases} \tag{28}$$

Together with the negative-sequence current as indicated in Equation (28), the oscillating parts of the extended reactive power are calculated as,

$$Q_{s_exi2} = 1.5 U_{s+} I_{s-} \sin\left(2\omega_g t + \theta_{u+} - \theta_{i-}\right) = 1.5 U_{s-} I_{s+} \sin\left(-2\omega_g t + \theta_{u-} - \theta_{i+}\right) = -Q_{s_exu2} \tag{29}$$

As seen, the oscillating parts of the extended reactive powers are opposite under such case. In other words, if Target I is active with constant classical active power, the extended reactive power is also controlled to be constant. It means that both the oscillating parts of the classical active power and the extended reactive power can be eliminated at the same time.

Notably, since the power reference has no pulsations, it is required that the power feedbacks are also non-oscillating. Meanwhile, for ensuring the average power delivery, the average parts of the power feedbacks are required to be equal to those of the classical active and reactive powers. Thus, based on the previous analysis, for achieving Target I, the power feedbacks are designed as,

$$\begin{cases} P_{sfb} = P_s \\ Q_{sfb} = Q_{s_ex} \end{cases} \tag{30}$$

If the designed power feedbacks are well controlled to track their references, the oscillating parts of the classical active power and the extended reactive power are eliminated simultaneously under unbalanced grid voltage conditions.

As for Target II, the oscillating reactive power is required to be removed, thus, the reactive power is controlled to be constant with no reactive power pulsations, i.e., $Q_{s_i2} + Q_{s_u2} = 0$. As indicated in [21], the oscillating part of the electromagnetic torque is proportional to that of the reactive power only with the unbalanced voltage. Consequently, with Target II enabled, both the oscillating parts of the reactive power and the electromagnetic torque can be eliminated simultaneously.

For achieving the fact that $Q_{s_i2} + Q_{s_u2} = 0$, based on (6), the amplitude and phase angle of the negative-sequence current are obtained as,

$$\begin{cases} I_{s-} = U_{s-} I_{s+} / U_{s+} \\ \theta_{i-} = \theta_{u+} - \theta_{i+} + \theta_{u-} \end{cases} \tag{31}$$

According to Equation (31), the oscillating part of the extended active power is expressed as,

$$P_{s_exi2} = 1.5 U_{s+} I_{s-} \cos\left(2\omega_g t + \theta_{u+} - \theta_{i-}\right) = 1.5 U_{s-} I_{s+} \cos\left(-2\omega_g t + \theta_{u-} - \theta_{i+}\right) = -P_{s_exu2} \tag{32}$$

As seen, when Target II is enabled, the constant extended active power is obtained, because the sum of the oscillating parts of the extended active powers is zero. It means that both the constant extended active power and the constant classical reactive power can be simultaneously obtained. As a result, for removing the oscillating reactive powers, the power feedbacks can be set as,

$$\begin{cases} P_{sfb} = P_{s_ex} \\ Q_{sfb} = Q_s \end{cases} \tag{33}$$

Notably, based on Equation (12), the average values of the extended and classical powers are equal to each other. Although the extended active power replaces the classical active power as the power feedback, the average power can be well regulated. If the negative-sequence current is properly injected as required by Equation (31), the oscillating parts of the extended active power and classical reactive power can be controlled to be constant.

For Target III, since the stator current is controlled to be balanced, the negative-sequence current is eliminated. Accordingly, the oscillating parts of the classical active and reactive powers caused by the negative-sequence current and positive-sequence voltage is zero, i.e., $P_{s_i2} = Q_{s_i2} = 0$. However, the oscillating parts caused by the negative-sequence voltage and the positive-sequence current still exist, i.e., $P_{s_u2} \neq 0$ and $Q_{s_u2} \neq 0$.

As analyzed previously, the oscillating classical and extended active/reactive powers are always opposite regardless of the negative-sequence current. Then, by adding the classical and extended powers, the constant power feedbacks are obtained. However, the average parts of the sums are twice the constant power references. Thus, for guaranteeing the average power delivery, an additional coefficient (0.5) needs to be inserted and then the power feedbacks are calculated as,

$$\begin{cases} P_{sfb} = 0.5(P_{s_ex} + P_s) \\ Q_{sfb} = 0.5(Q_{s_ex} + Q_s) \end{cases} \tag{34}$$

3.2. System Implementation

Based on the previous analysis, the power feedback contains both the average part and the oscillating part with twice the grid frequency under unbalanced grid voltage conditions. In other words, for effectively tracking the constant power references with zero steady-state errors, the power controller is required to regulate both DC signals and ac signals at twice the grid frequency. Consequently, the widely-used ac controller, i.e., PI+R controller tuned at twice the grid frequency, is employed in this VM-DPC strategy to regulate the power feedbacks to track their corresponding references.

It is noted that there is an allowed frequency deviation in a narrow range around the nominal frequency [24,25]. In order to reduce the sensitivity of frequency deviations and guarantee the stable operation over frequency deviations around the nominal frequency, in practical applications, a cutoff frequency ω_c = 5–20 rad/s is inserted as a damping factor. Thus, the complete expression of the employed power controller is given as,

$$G(s) = k_p + \frac{k_i}{s} + \frac{2k_r\omega_c s}{s^2 + 2\omega_c s + (2\omega_1)^2} \tag{35}$$

where k_p, k_i and k_r are the proportional, integral and resonant parameters, ω_c is the cutoff frequency and set as 10 rad/s, respectively.

According to Equation (27), the modulated voltages of the active and reactive powers are obtained by,

$$\begin{cases} u_P = \underbrace{\frac{2}{3}v_P}_{\text{feedback}} + \underbrace{\frac{2\sigma L_r L_s}{3L_m}(\omega_1 P_{s_ex} + \omega_r Q_s) - \omega_r\left(u_{s\beta}\psi_{s\alpha} + u_{s\alpha}\psi_{s\beta}\right)}_{\text{feedforward}} \\ u_Q = \underbrace{\frac{2}{3}v_Q}_{\text{feedback}} + \underbrace{\frac{2\sigma L_r L_s}{3L_m}(\omega_1 Q_{s_ex} - \omega_r P_s) - \omega_r\left(u_{s\alpha}\psi_{s\alpha} - u_{s\beta}\psi_{s\beta}\right)}_{\text{feedforward}} \end{cases} \tag{36}$$

where v_P and v_Q are the outputs of the power controllers,

$$\begin{cases} v_P = G(s) \cdot (P_{sref} - P_{sfb}) \\ v_Q = G(s) \cdot (Q_{sref} - Q_{sfb}) \end{cases} \tag{37}$$

where P_{sref} and Q_{sref} are the active and reactive power references, P_{sfb} and Q_{sfb} are the active and reactive power feedbacks given in Equation (30), (33) and (34), respectively.

Accordingly, together with the PI+R controller and the feedforwards in Equation (36), the modulated voltages of the active and reactive powers are gotten. For obtaining the rotor voltage from the modulated voltage of the active and reactive powers, based on the generator model, the non-linear VM controller is designed as,

$$\begin{bmatrix} u_{r\alpha} \\ u_{r\beta} \end{bmatrix} = \frac{L_r}{L_m}\begin{bmatrix} u_{s\alpha} \\ u_{s\beta} \end{bmatrix} - \frac{1}{U_{sm}^2}\begin{bmatrix} u_{s\beta} & u_{s\beta} \\ u_{s\beta} & -u_{s\beta} \end{bmatrix}\begin{bmatrix} u_P \\ u_Q \end{bmatrix} \tag{38}$$

As seen, the rotor voltage can be easily obtained with a simple calculation. Then, the rotor voltage is transferred from the stator stationary reference frame to the rotor stationary one with Park Transformation based on the rotor position angle as,

$$\begin{bmatrix} u_{r\alpha_r} \\ u_{r\beta_r} \end{bmatrix} = \begin{bmatrix} \cos\theta_r & \sin\theta_r \\ -\sin\theta_r & \cos\theta_r \end{bmatrix}\begin{bmatrix} u_{r\alpha} \\ u_{r\beta} \end{bmatrix} \tag{39}$$

where $u_{r\alpha_r}$ and $u_{r\beta_r}$ are the required rotor voltages in the rotor stationary reference frame, θ_r is the rotor position angle, respectively.

Figure 2 gives the block diagram of the developed VM-DPC strategy. Since the delay unit for obtaining the one-quarter-of-fundamental-period delayed stator voltage is not in the scope of this paper, a simple $T/4$-delay method is employed in the control system, where T = 20 ms is the fundamental period. As seen, the VM-DPC consists of three parts: (1) the power feedback generation that provides the available power feedback for achieving the defined control targets; (2) the power tracking control that guarantees the power feedback to track its reference with the conventional PI+R controller and feedforwards; (3) the VM controller that generates the rotor voltage from the modulated voltage of the active and reactive powers.

In the VM-DPC strategy, the extended active and reactive powers are calculated in Equation (9) based on the delayed voltage and the measured currents. Together with the classical active and reactive powers in Equation (4), three power feedbacks are designed as shown in Equation (30), (33) and (34) for the achievement of the constant active power, the constant reactive power and the balanced stator current under unbalanced grid voltage conditions. Together with the conventional PI+R controller and feedforwards, the power feedbacks are well controlled to track their references with the proper modulated voltages. Then, the non-linear VM controller is employed to obtain the rotor voltage from

the modulated voltage. Finally, based on the rotor voltages, the SVM technique is introduced to generate the switching voltage vectors with their respective duration times.

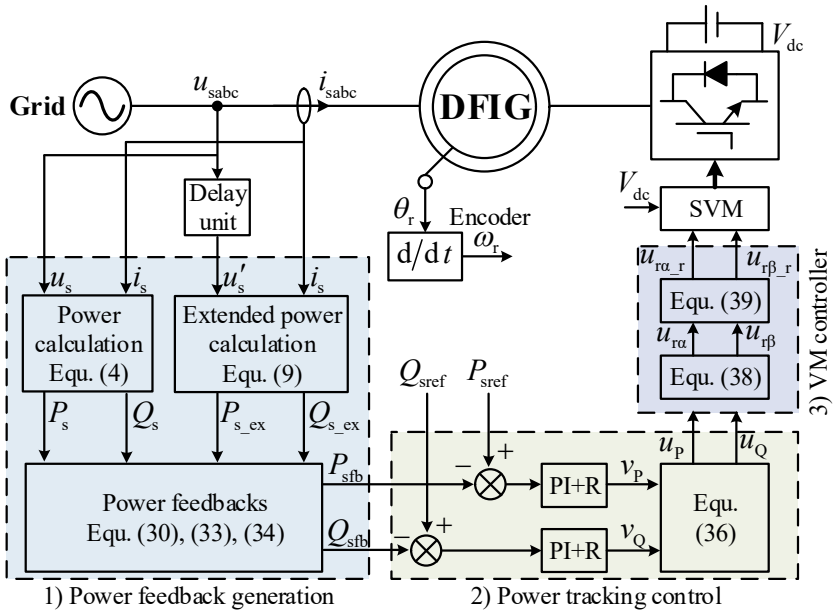


Figure 2. Block diagram of the developed voltage modulated direct power control (VM-DPC) strategy.

By these means, the generator is adequately controlled to achieve the predefined control targets with enhanced behavior. As seen from Figure 2, all the calculations and implementations are carried out in the stationary reference frame with no PLL. The introduction of the modulated voltage of the active and reactive power and the non-linear VM controller causes the power dynamics to be the time-invariant ones, which enables the easy application of various control methods. Meanwhile, compared to the existing solutions in [19–21], the sequence extractions and the power compensations are not essential here, thereby resulting in a simpler implementation.

4. Simulation Studies

To validate the effectiveness of the proposed VM-DPC strategy, simulation studies were conducted using Matlab/Simulink, and Figure 3 shows the schematic diagram of the simulated system. The generator was rated at 2.0 MW with its parameters given in Table 1. The nominal DC-link voltage was fixed at 1100 V. The grid-side converter was used to maintain the constant DC-link voltage and was controlled by a conventional method of PWM rectifiers, which is not included in this paper. During the simulations, a switching frequency of 3.0 kHz was used in the developed VM-DPC strategy. The rotor speed was initially set at 1.2 p.u. (super-synchronous), because the mechanical time constant is much larger than the electromagnetic one. Besides, an additional three-phase programmable voltage source was used to provide the unbalanced grid with a larger voltage unbalance being 10%. In the following tests, four different operating modes were adopted and compared.

(1) Mode I: the classical active and reactive powers in Equation (4) are set as the feedback powers.
(2) Mode II: the classical active power and the extended reactive power in Equation (30) are set as the feedback powers.
(3) Mode III: the extended active power and the classical reactive power in Equation (33) are set as the feedback powers.
(4) Mode IV: the calculated active and reactive powers based on the classical and extended powers in Equation (34) are set as the feedback powers.

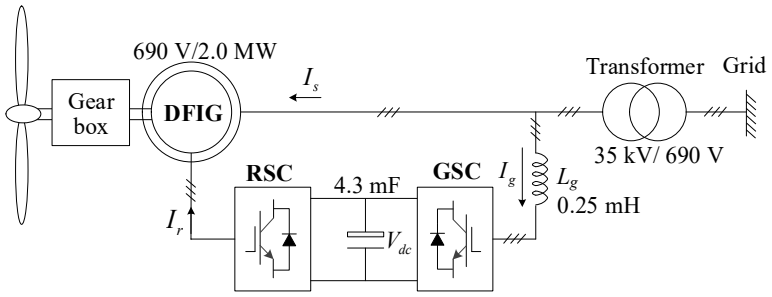


Figure 3. Schematic diagram of the simulated system.

Table 1. Parameters of the simulated DFIG.

Parameter	Value	Parameter	Value
Rated power	2.0 MW	Rated voltage	690 V
R_s	0.0083 p.u.	DC voltage	1100 V
R_r	0.0069 p.u.	$L_{\delta s}$	0.090 p.u.
L_m	4.810 p.u.	$L_{\delta r}$	0.065 p.u.
Stator/rotor turns ratio	0.33	Pole number	4
k_p	20	k_i	40
k_r	500	ω_c	10

Figure 4 gives the simulation results of the tested DFIG during active and reactive power steps. Since the positive direction of the stator current is into the generator, the negative active power refers to the power delivered from the generator to the grid. Meanwhile, the negative reactive power refers to the capacitive reactive power. In this test, the stator active and reactive powers were initially set at −0.5 p.u. and 0.0 p.u., respectively. The active power reference was changed to −0.8 p.u. at 0.1 s and then back to −0.5p.u. at 0.5 s. The reactive power reference was changed to −0.2 p.u. at 0.2 s and then back to 0 p.u. at 0.4 s. Since there was no voltage unbalance, both the classical and extended powers were constant with no oscillating parts and they were equal to each other. Thus, in this test, the classical active and reactive powers were set as the power feedbacks with Mode I enabled. As seen, during the active and reactive power steps, the stator active and reactive powers can effectively track their references with zero steady-state errors. The active and reactive powers can also achieve a decoupling regulation. During the power steps, the stator and rotor current remained highly sinusoidal with their total harmonic distortions (THDs) being 2.3% and 2.2%, respectively. Therefore, the VM-DPC strategy can guarantee good tracking during power changes and the decoupling regulation between the active and reactive powers.

Figure 5 gives the simulation results during a 10% transient voltage unbalance, where the stator active and reactive powers are set at −1.0 p.u. and 0.0 p.u., respectively. In this test, the developed VM-DPC strategy applied the classical active and reactive powers to be the feedbacks. As seen, in this mode, the stator active and reactive powers are controlled to be constant with no oscillating parts. However, the stator current was highly distorted with obvious third harmonic components of 150 Hz being 9.8%. Since the rotor rotates at 60 Hz in the positive direction, the third stator current introduces 90 Hz rotor harmonic current in the rotor winding, which is around 9.9%. The THDs of the stator and rotor currents were as much as 10.2% and 10.3%, respectively. Meanwhile, the electromagnetic torque oscillated badly and contained an oscillating part equivalent to 19.5%. As seen, the developed VM-DPC with the classical powers of the power feedbacks cannot guarantee satisfactory behaviors under unbalanced grid voltage conditions.

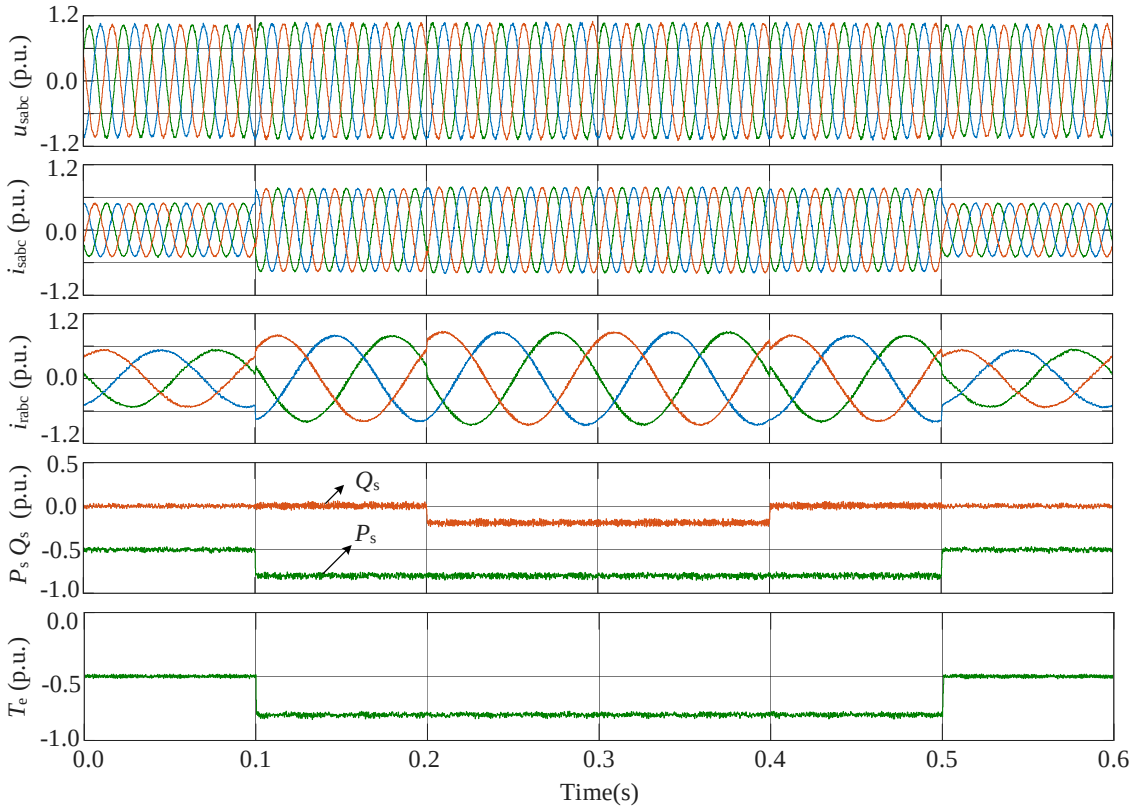


Figure 4. Simulation results during the power steps under balanced grid voltage conditions.

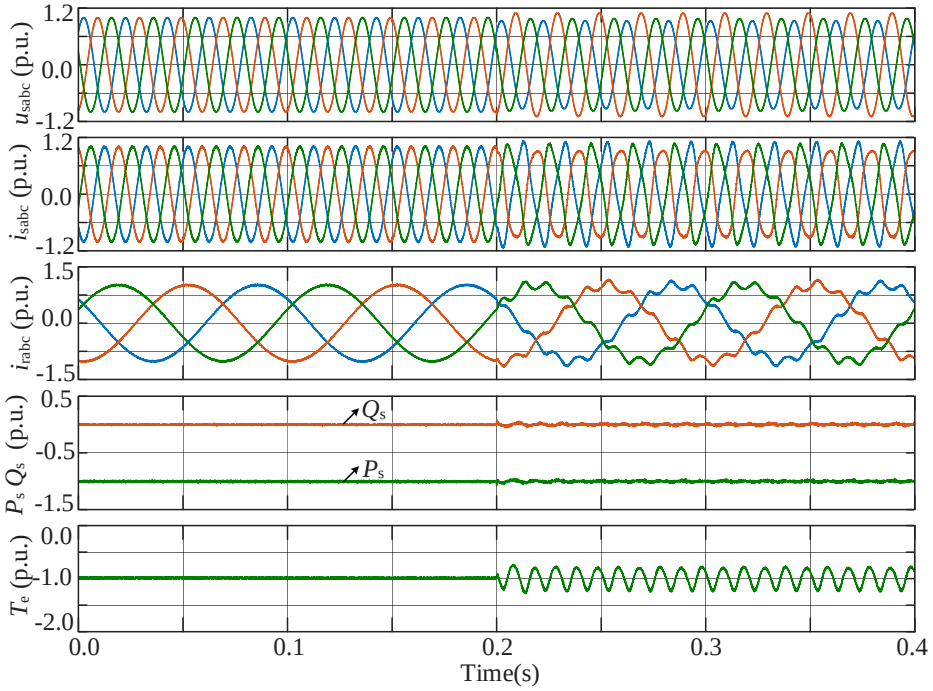


Figure 5. Simulation results during a 10% transient voltage unbalance.

Figure 6 gives the simulation results during a 10% steady-state voltage unbalance, where the following four different operating modes are compared. As seen from Figure 6, under Mode I, the stator active and reactive powers are controlled to be non-oscillating, but the stator currents are highly distorted, as analyzed previously. When the feedback powers are switched to (30) under Mode II at 0.2 s,

the harmonic components of the stator currents are immediately eliminated. The stator currents are highly sinusoidal with the THD being 1.8%. The current unbalance factor (CUF) of the stator current, referring to the radio of the amplitude of the negative-sequence current to that of the positive-sequence current, is around 10.8%. The stator active power remains constant, while the reactive power contains an oscillating part equal to 19.8%. Consequently, Target I of removing the oscillating active power was achieved. At 0.4 s, the control system was switched to Mode III with Target II enabled. Under such a case, the oscillating part of the reactive power is removed as expected. Notably, since the oscillating part of the electromagnetic torque is proportional to that of the stator reactive power only with the positive- and negative-sequence current injection [21], under Mode III, the oscillating parts of the electromagnetic torque can also be eliminated. The oscillating part of the stator active power was increased to around 19.2%. Under this mode, the CUF of the stator current was 9.1%, while its THD was about 1.8%. When Mode IV was enabled at 0.6 s, the CUF of the stator current immediately decreased to 0.1%, where Target III of guaranteeing the balanced stator current was achieved. The THDs of the stator and rotor currents were 1.7% and 2.1%, respectively. The active and reactive powers contained the oscillating parts of 9.3% and 9.6%, respectively. Besides, the amplitude of the torque ripples was around 11.4%. Thus, by the means of applying different power feedbacks, the predefined control targets were achieved with enhanced behaviors, which can provide the enhanced behaviors under unbalanced grid voltage conditions.

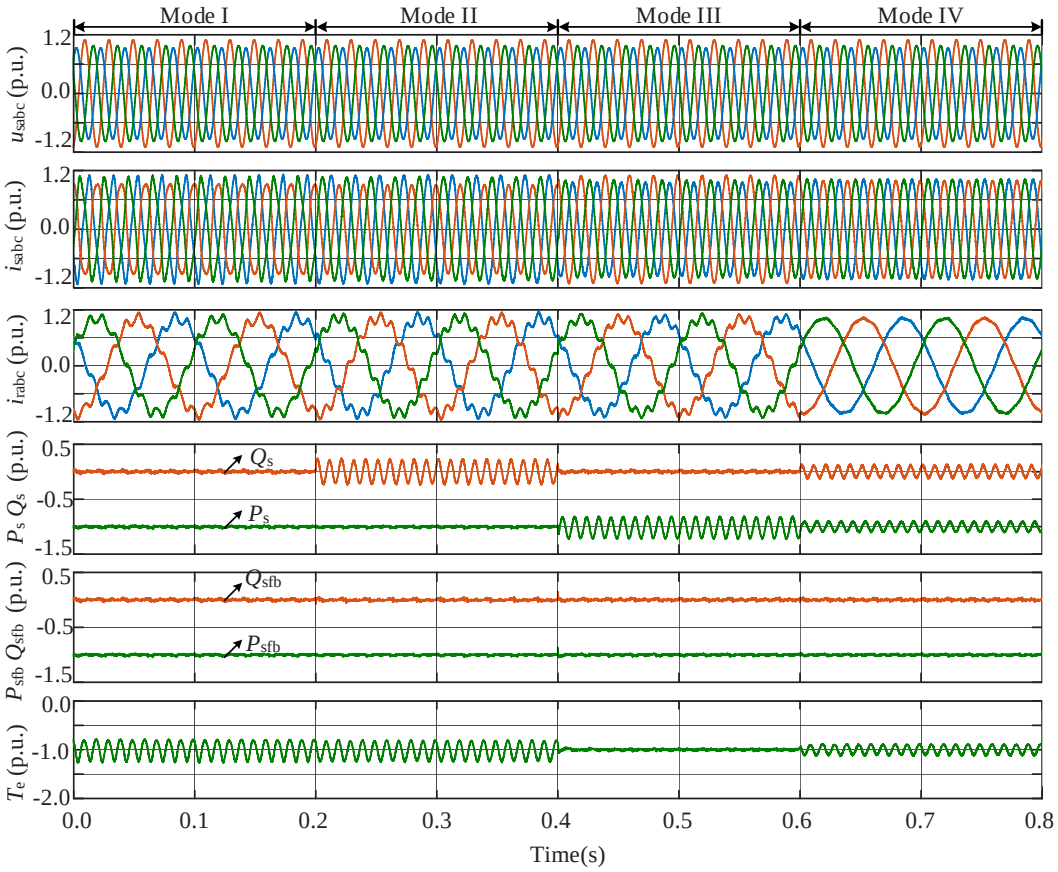


Figure 6. Simulation results during a 10% steady-state voltage unbalanc.

For clear comparisons, Table 2 summarizes the THD of the stator current, the CUF of the stator current, and the oscillating amplitude of the active power, the reactive power, and the electromagnetic torque among different operating modes. It is evident that the developed VM-DPC, with the available

power feedbacks, can greatly enhance and improve the generator performance under unbalanced grid voltage conditions.

Table 2. Comparisons among different modes during network unbalance.

	Mode I	Mode II	Mode III	Mode IV
i_{sabc} total harmonic distortion (%)	10.2	1.8	1.8	1.7%
i_{sabc} current unbalance factor (%)	1.1	10.8	9.1	0.1
P_s oscillation (%)	0.4	0.4	19.2	9.3
Q_s oscillation (%)	0.4	19.8	0.4	9.6
T_e oscillation (%)	19.5	19.4	0.4	11.4

Figure 7 gives further simulation results with Mode II enabled during a 10% transient voltage unbalance. In this test, the generator was controlled to remove the oscillating part of the stator active power. The active and reactive powers of the DFIG were fixed at −1.0 p.u. and 0.0 p.u, which is the same as those of Figures 5 and 6. As seen, at 0.2 s, when a 10% transient voltage unbalance arises, the feedback powers can rapidly track the commanded values in around 20 ms. Meanwhile, the oscillating parts of the stator active power are eliminated with highly sinusoidal current provisions. Consequently, the developed VM-DPC strategy can provide fast dynamic responses during a transient unbalance.

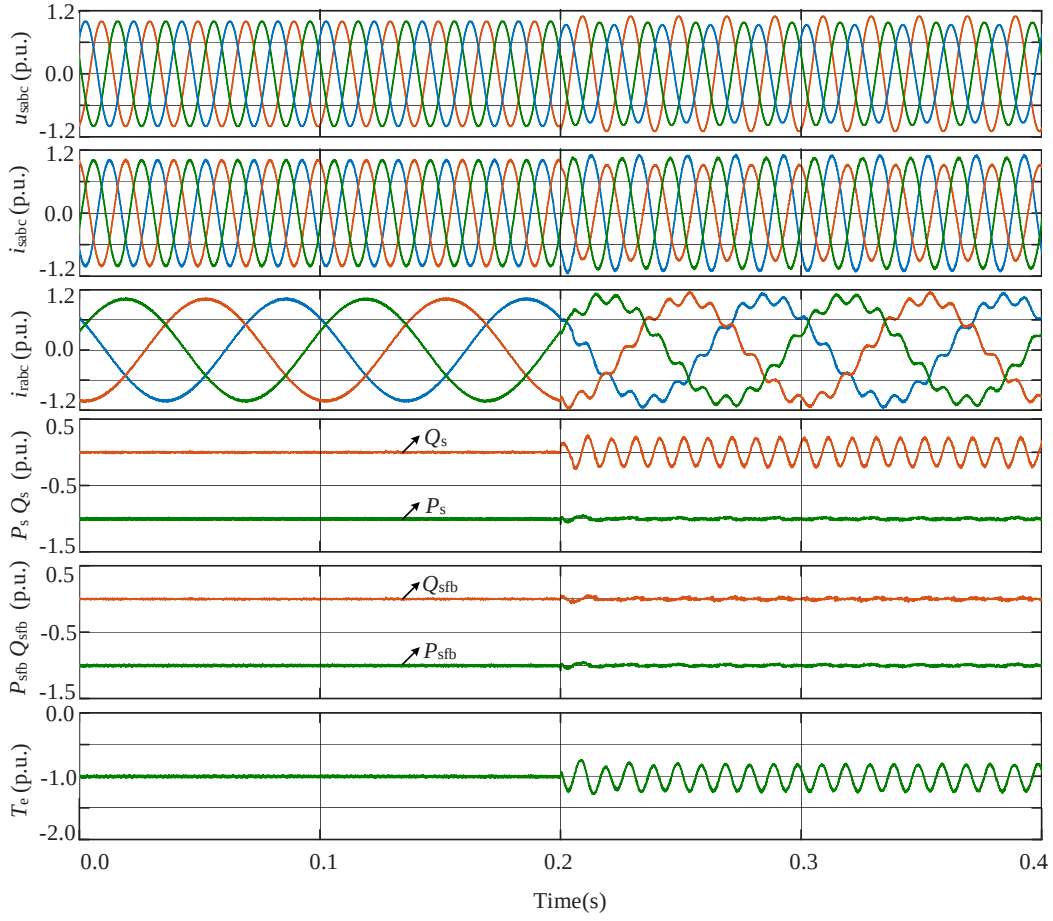


Figure 7. Simulation results with Mode II enabled during a 10% transient voltage unbalance.

As a result, based on the aforementioned simulation results, it is confirmed that the proposed VM-DPC with different power feedbacks can achieve the predefined control targets and provide

both satisfactory steady-state performance and suitable dynamic behaviors under unbalanced grid voltage conditions.

5. Conclusions

This paper describes a developed VM-DPC strategy of DFIGs using the extended power theory under unbalanced grid voltage conditions. It introduces the modulated voltage of the active and reactive powers and the non-linear VM controller in this proposed strategy. Accordingly, the differential equations describing the power dynamics of the generator change from the time-varying system to the time-invariant one. Then, in order to deal with the voltage unbalance, the proposed VM-DPC strategy combines the classical and extended power to generate the available power feedbacks. Then, the generated power feedbacks are well regulated by the conventional controller (PI+R controller and feedforwards) and the non-linear VM controller with the achievement of the predefined control targets. Compared to the existing solutions, the main advantage of the developed VM-DPC strategy can be summarized as: (1) the induction of the modulated voltage of the active and reactive powers and the non-linear VM controller that causes the power dynamics to be the time-invariant ones for easily applying various control methods; (2) the lack of the sequence extractions and the power compensations for achieving the control targets under unbalanced grid voltage conditions. Finally, the simulation results are provided to validate the effectiveness of the developed VM-DPC strategy. Since the grid impedance is not considered in this paper, the weak grid condition will be considered in future work to make a robust control strategy even under weak grid conditions.

Author Contributions: Conceptualization, P.C. and C.W.; methodology, P.C.; software, F.N. and J.H.; validation, P.C., F.N. and J.H.; formal analysis, P.C.; investigation, P.C. and C.W.; resources, P.C.; data curation, P.C. and C.W.; writing—original draft preparation, P.C.; writing—review and editing, P.C. and C.W.; visualization, P.C.; supervision, P.C.; project administration, P.C.; funding acquisition, P.C. All authors have read and agreed to the published version of the manuscript.

Funding: This research was funded by the Science and Technology Project of State Grid Corporation of China under Grant NYB17201900282.

Conflicts of Interest: The authors declare no conflict of interest.

References

1. Blaabjerg, F.; Ma, K. Wind energy systems. *Proc. IEEE* **2017**, *105*, 2116–2131.
2. Yaramasu, V.; Wu, B.; Sen, P.; Kouro, S.; Narimani, M. High-power wind energy conversion systems: State-of-the-art and emerging technologies. *Proc. IEEE* **2015**, *103*, 740–788. [CrossRef]
3. Jia, J.; Yang, G.; Nielsen, A.H. A review on grid-connected converter control for short-circuit power provision under grid unbalanced faults. *IEEE Trans. Power Deliv.* **2018**, *33*, 649–661. [CrossRef]
4. Wang, T.; Kong, L.; Nian, H.; Zhu, Z.Q. Coordinated elimination strategy of low order output current distortion for LC-filtered DFIG system based on hybrid virtual impedance method. *IEEE Trans. Power Electron.* **2019**, *34*, 7502–7520. [CrossRef]
5. Shuai, Z.; Xiao, M.; Ge, J.; Shen, Z.J. Overcurrent and its restraining method of PQ-controlled three-phase four-wire converter under asymmetrical grid fault. *IEEE J. Emerg. Sel. Top. Power Electron.* **2019**, *7*, 2057–2069. [CrossRef]
6. Mahamedi, B.; Eskandari, M.; Fletcher, J.E.; Zhu, J. Sequence-based control strategy with current limiting for the fault ride-through of inverter-interfaced distributed generators. *IEEE Trans. Sustain. Energy* **2020**, *11*, 165–174. [CrossRef]
7. Golestan, S.; Guerrero, J.M.; Vasquez, J.C. Three-phase PLLs: A review of recent advances. *IEEE Trans. Power Electron.* **2017**, *32*, 1897–1907. [CrossRef]
8. Zhu, D.; Zhou, S.; Zou, X.; Kang, Y. Improved design of PLL controller for LCL-type grid-connected converter in weak grid. *IEEE Trans. Power Electron.* **2020**, *35*, 4715–4727. [CrossRef]
9. Liu, J.; Yao, W.; Wen, J.; Fang, J.; Jiang, L.; He, H.; Cheng, S. Impact of power grid strength and PLL parameters on stability of grid-connected DFIG wind farm. *IEEE Trans. Sustain. Energy* **2020**, *11*, 545–557. [CrossRef]

10. Shabestary, M.M.; Mohamed, Y.R.I. Asymmetrical ride-through and grid support in converter-interfaced DG units under unbalanced conditions. *IEEE Trans. Ind. Electron.* **2019**, *66*, 1130–1141. [CrossRef]
11. Afshari, E.; Moradi, G.R.; Rahimi, R.; Farhangi, B.; Yang, Y.; Blaabjerg, F.; Farhangi, S. Control strategy for three-phase grid-connected PV inverters enabling current limitation under unbalanced faults. *IEEE Trans. Ind. Electron.* **2017**, *64*, 8908–8918. [CrossRef]
12. Taul, M.G.; Wang, X.; Davari, P.; Blaabjerg, F. Current reference generation based on next generation grid code requirements of grid-tied converters during asymmetrical faults. *IEEE J. Emerg. Sel. Top. Power Electron.* **2019**. [CrossRef]
13. Guo, X.Q.; Liu, W.; Zhang, X.; Sun, X.; Lu, Z.; Guerrero, J.M. Flexible control strategy for grid-connected inverter under unbalanced grid faults without PLL. *IEEE Trans. Power Electron.* **2015**, *30*, 1773–1778. [CrossRef]
14. Zhang, Y.; Jiao, J.; Xu, D.; Jiang, D.; Wang, Z.; Tong, C. Model predictive direct power control of doubly fed induction generators under balanced and unbalanced network conditions. *IEEE Trans. Ind. Appl.* **2020**, *56*, 771–786. [CrossRef]
15. Zhou, D.; Tu, P.; Tang, Y. Multi-vector model predictive power control of three-phase rectifiers with reduced power ripples under non-ideal grid conditions. *IEEE Trans. Ind. Electron.* **2018**, *65*, 6850–6859. [CrossRef]
16. Wang, X.; Sun, D. Three-vector-based low-complexity model predictive direct power control strategy for doubly fed induction generators. *IEEE Trans. Power Electron.* **2017**, *32*, 773–782. [CrossRef]
17. Zhang, Y.; Jiao, J.; Xu, D. Direct power control of doubly fed induction generator using extended power theory under unbalanced network. *IEEE Trans. Power Electron.* **2019**, *34*, 12024–12037. [CrossRef]
18. Li, L.; Nian, H.; Ding, L.; Zhou, B. Direct power control of DFIG system without phase-locked loop under unbalanced and harmonically distorted voltage. *IEEE Trans. Energy Convers.* **2018**, *33*, 395–405. [CrossRef]
19. Kabiri, R.; Holmes, D.G.; Mcgrath, B.P. Control of active and reactive power ripple to mitigate unbalanced grid voltages. *IEEE Trans. Ind. Appl.* **2016**, *52*, 1660–1668. [CrossRef]
20. Nian, H.; Shen, Y.; Yang, H.; Quan, Y. Flexible grid connection technique of voltage-source inverter under unbalanced grid conditions based on direct power control. *IEEE Trans. Ind. Appl.* **2015**, *51*, 4041–4050. [CrossRef]
21. Sun, D.; Wang, X.; Nian, H.; Zhu, Z.Q. A sliding-mode direct power control strategy for DFIG under both balanced and unbalanced grid conditions using extended active power. *IEEE Trans. Power Electron.* **2017**, *33*, 1313–1322. [CrossRef]
22. Gui, Y.; Li, M.; Lu, J.; Golestan, S.; Guerrero, J.M.; Vasquez, J.C. A voltage modulated DPC approach for three-phase PWM rectifier. *IEEE Trans. Ind. Electron.* **2018**, *65*, 7612–7619. [CrossRef]
23. Gui, Y.; Kim, C.; Chung, C.; Guerrero, J.M.; Guan, Y.J.; Vasquez, J.C. Improved direct power control for grid-connected voltage source converters. *IEEE Trans. Ind. Electron.* **2018**, *65*, 8041–8051. [CrossRef]
24. *Power Quality-Frequency Deviation for Power System*; Chinese National Standard GB/T 15945-2008; Standardization Administration of the PRC: Beijing, China, 2008.
25. *Compatibility Levels for Low-Frequency Conducted Disturbances and Signaling in Public Low-Voltage Power Supply System*; IEC 61000-2-2-2002; International Electrotechnical Commission: Geneva, Switzerland, 2002.

Publisher's Note: MDPI stays neutral with regard to jurisdictional claims in published maps and institutional affiliations.

© 2020 by the authors. Licensee MDPI, Basel, Switzerland. This article is an open access article distributed under the terms and conditions of the Creative Commons Attribution (CC BY) license (http://creativecommons.org/licenses/by/4.0/).